Journal of Colloid and Interface Science 635 (2023) 552–561

Contents lists available at ScienceDirect

Journal of Colloid and Interface Science

journal homepage: www.elsevier.com/locate/jcis

In situ single particle characterization of the themoresponsive and co-nonsolvent behavior of PNIPAM microgels and silica@PNIPAM core-shell colloids

Albert Grau-Carbonell *, Fabian Hagemans, Maarten Bransen, Nina A. Elbers, Relinde J.A. van Dijk-Moes, Sina Sadighikia, Tom A.J. Welling, Alfons van Blaaderen *, Marijn A. van Huis *

Soft Condensed Matter, Debye Institute for Nanomaterials Science, Utrecht University, Princetonplein 1, Utrecht 3584 CC, the Netherlands

HIGHLIGHTS

- PNIPAM microgels were imaged via liquid cell electron microscopy.
- The thermoresponsive and co-nonsolvent behavior of PNIPAM was followed.
- Beam effects as well as their mitigation via radical scavengers are discussed.

GRAPHICAL ABSTRACT

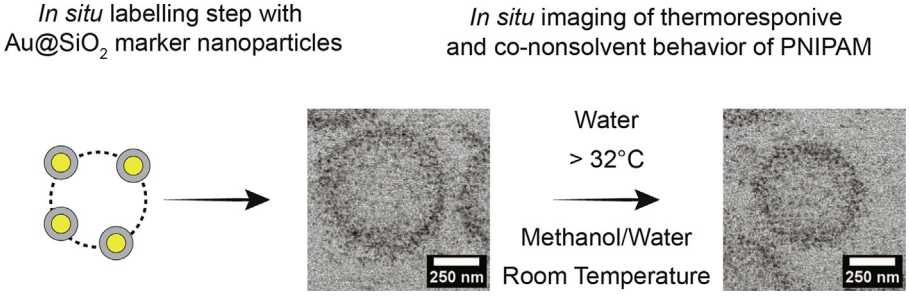

ARTICLE INFO

Article history:
Received 28 October 2022
Revised 15 December 2022
Accepted 20 December 2022
Available online 24 December 2022

Keywords:
Liquid Cell STEM
PNIPAM
Thermoresponsive behavior
Co-nonsolvent behavior

ABSTRACT

Poly(N-isopropylacrylamide) (PNIPAM) microgels and PNIPAM colloidal shells attract continuous strong interest due to their thermoresponsive behavior, as their size and properties can be tuned by temperature. The direct single particle observation and characterization of pure, unlabeled PNIPAM microgels in their native aqueous environment relies on imaging techniques that operate either at interfaces or in cryogenic conditions, thus limiting the observation of their dynamic nature. Liquid Cell (Scanning) Transmission Electron Microscopy (LC-(S) TEM) imaging allows the characterization of materials and dynamic processes such as nanoparticle growth, etching, and diffusion, at nanometric resolution in liquids. Here we show that via a facile post-synthetic *in situ* polymer labelling step with high-contrast marker core–shell Au@SiO_2 nanoparticles (NPs) it is possible to determine the full volume of PNIPAM microgels in water. The labelling allowed for the successful characterization of the thermoresponsive behavior of PNIPAM microgels and core shell silica@PNIPAM hybrid microgels, as well as the co-nonsolvency of PNIPAM in aqueous alcoholic solutions. The interplay between electron beam irradiation and PNIPAM systems in water resulted in irreversible shrinkage due to beam induced water radiolysis products, which in turn also affected the thermoresponsive behavior of PNIPAM. The addition of 2-propanol as radical scavenger improved PNIPAM stability in water under electron beam irradiation.

1. Introduction

Thermoresponsive microgels are of great interest because of their widely reported rheological, biomedical, optical, catalytic and chemical sensing applications [1–5]. These systems undergo

* Corresponding authors.
E-mail addresses: A.GrauCarbonell@gmail.com (A. Grau-Carbonell), A.vanBlaaderen@uu.nl (A. van Blaaderen), M.A.vanHuis@uu.nl (M.A. van Huis).

https://doi.org/10.1016/j.jcis.2022.12.116
0021-9797/

an abrupt change in aqueous solubility when heated above a temperature threshold, known as the lower critical solution temperature (LCST). Poly(N-isopropylacrylamide) (PNIPAM) was one of the first reported thermoresponsive polymers and has since then been the base for a vast number of thermoresponsive microgels. [6] PNIPAM, and PNIPAM based microgels, exhibit a characteristic LCST of around 32 °C in water which is easily tunable with the incorporation of different comonomers. [7] Below this LCST, microgels are soluble in water and are found in a swollen state. Upon heating above the LCST the hydrogen bonds that are keeping the polymer chains fully solvated, are disrupted and a well-defined and reversible conformational transformation from well-solvated coils to a globular state takes place [8]. PNIPAM microgels can be functionalized not only by changing the chemistry of the polymer but by forming more complex hybrid structures. These hybrid structures range for instance from hollow microgels to core@shell systems with nanoparticles (NPs) to complex multi-shelled microgels. [3] These more complex hybrid PNIPAM particles systems have a broad range of applications such as temperature tunable depletants and drug delivery vessels that can release chemicals upon temperature changes. [9] Moreover, PNIPAM shows an interesting and still not fully understood co-nonsolvent behavior in alcoholic aqueous solutions [10]. PNIPAM polymers are well-solvated in pure water or alcohols (i.e. methanol, propanol) but undergo a coil-to-globe transition for mixtures of both solvents. [10,11].

Despite decades of advancements in the synthesis and application of microgels, their complete characterization is still lacking. A wide toolkit of characterization techniques has been developed regarding many properties of the microgels, and thus PNIPAM as well [12]. Scattering techniques have been exploited to study microgels with nanometric resolving power, yielding radially averaged properties of ensembles of particles. Dynamic Light Scattering (DLS) in particular has been most often used to characterize the temperature dependent hydrodynamic radius of microgels and thus the themoresponsive behavior of PNIPAM microgels [13]. However, scattering measurements rely on models of the scattering units and these are only straightforward to obtain for spherically symmetric, and homogeneous systems and therefore scattering techniques are limited in analyzing quantitatively the thermoresponsive behavior of anisotropic, deformed, or otherwise more complex microgels. Atomic Force Microscopy (AFM) measurements, although constrained to particles on surfaces or adsorbed to interfaces, have been able to follow themoresponsive microgel behavior at the single particle level, as well as revealing microgel internal features (i.e. the presence of humps on the surface of the microgels even in their most collapsed state) [14]. Light microscopy and light nanoscopy techniques have also been used to image microgels [15,16]. Light nanoscopy or super-resolution techniques such as stochastic optical reconstruction microscopy (STORM) have shown great success in imaging single particles and studying their internal structure with sub-diffraction resolutions. [17] Even higher resolution in the direct imaging of single microgels can be achieved with electron microscopy (EM), which is of particular interest to study hybrid microgels in which the microgel is a thin shell around a nanoparticle (not necessarily with a trivial geometry). Cryo-EM (EM imaging of snap-frozen samples) has been able to determine the thermoresponsive behavior of core–shell polystyrene-PNIPAM particles [18,19]. However, Cryo-EM in microgel characterization is often somewhat limited by the unknown effects of the rapid cooling and blotting on polymer conformations, as well as the difficult preparation of Cryo-EM specimens.

In this study we report the successful characterization *in situ* of the thermoresponsive and co-nonsolvent behavior of PNIPAM microgels in their native water environment with nanometric resolution via liquid cell (scanning) transmission electron microscopy (LC-(S) TEM). In LC-(S) TEM, a thin volume of liquid (up to a few microns) is encapsulated and sealed, typically between two silicon chips harboring two opposing silicon nitride windows (Si_xN_y, 30–50 nm thickness) for imaging. These samples are able to withstand the high vacuum inside a TEM and can be imaged with conventional TEM and (S) TEM techniques. LC samples are loaded in dedicated TEM holders, typically equipped with microfluidic, heating and electrochemistry capabilities [20–22]. The main limitations of LC-(S) TEM are the limits in resolution imposed by the liquid layer thickness, as well as the beam-solvent and particles interactions resulting in the formation of, amongst other chemical effects, reactive radiolysis radicals [23,24]. Efforts to characterize the thermoresponsive behavior of PNIPAM microgels have been reported via incorporation of nanoparticles in the polymeric matrix by chemical synthesis and subsequent imaging in water, but for such systems many concepts have not yet been explored such as electron-beam-sample interactions, reversibility of the phase transition [25]. Our approach uses an *in situ* post-synthetic labelling step of the PNIPAM microgels with high contrast marker particles, core@shell Au@silica NPs, that allow for the low dose imaging of even swollen microgels that would otherwise yield hardly detectable signals for doses that do not affect the thermoresponsive behavior. Our methodology allows for the direct imaging of previously unlabelled PNIPAM microgels without the need for additional synthetic steps. In order to come up with a good strategy for fully imaging the reversible thermoresponsive behavior of single particles, we extensively studied the effects of LC-(S) TEM to the imaging of PNIPAM microgels by evaluating electron beam effects, by exploring the role of radical scavengers on PNIPAM stability under irradiation in water and by testing the behavior of various potential marker NPs. Therefore, as order of topics for this work we will first discuss electron beam effects on PNIPAM microgels in water and how they can be minimized, after which the best strategy to image the microgels are explored. The knowledge obtained was then applied to the characterization *in situ* of PNIPAM microgels and their behavior under changing temperatures and solvent composition.

2. Results and discussion

2.1. PNIPAM microgels and characterization

In this study two microgel systems were studied. PNIPAM microgels were synthesized via radical emulsion polymerization in the presence of a cross-linker. Hybrid core–shell silica(SiO_2)@PNIPAM microgels, consisting of a SiO_2 core and a thin PNIPAM shell, were synthesized via radical emulsion polymerization of PNIPAM onto SiO_2 cores whose surface had been modified with a silane coupling agent that had a double bond and thus could be chemically attached to PNIPAM chains.

2.1.1. Dynamic light scattering and conventional TEM

The PNIPAM microgels showed, as measured via Dynamic Light Scattering (DLS), a hydrodynamic diameter at room temperature (RT, 21 °C) of D_{RT} = 650–670 nm, and a hydrodynamic diameter at temperatures above the LCST of around $D_{40°C}$ = 350–400 nm (**Fig. 1**A). Under our synthesis conditions, PNIPAM particles are known to consist of a core–shell structure with a more dense core with high a cross-linker density and a less dense corona [26–28]. This corona is mainly responsible for the thermoresponsive behavior of such structures [29–31]. Therefore, a structure having a core with a diameter corresponding to $D_{40°C}$ and a total size of core/-corona diameter of D_{RT} is expected. PNIPAM particles dried on a sil-

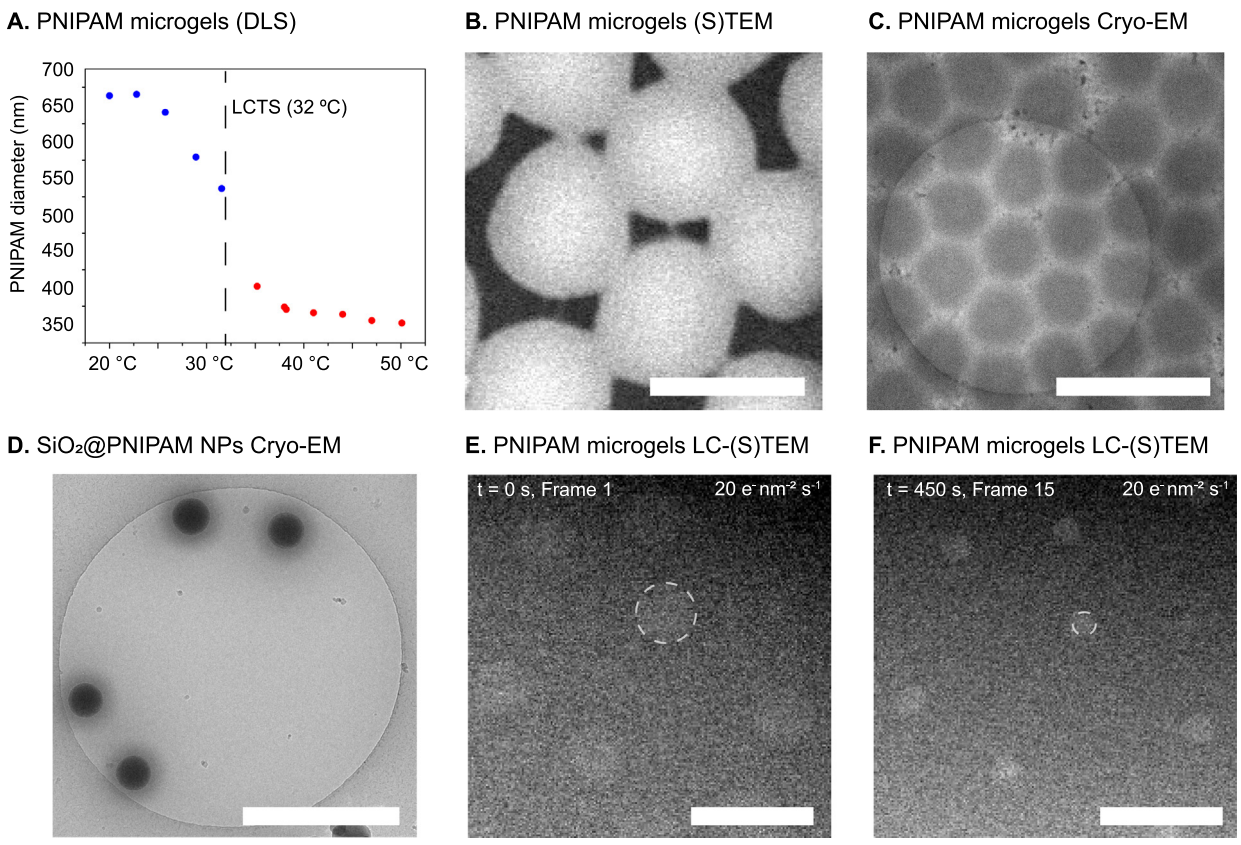

Fig. 1. Characterization of PNIPAM micorgels and SiO_2@PNIPAM nanoparticles (NPs). A. Hydrodynamic radius as determined with Dynamic Light Scattering (DLS) of PNIPAM microgels. The thermoresponsive behavior of PNIPAM is clearly visible as function of temperature, with the swollen size of D_{RT} = 650–670 nm when the system temperature is below the Lower Critical Solution Temperature (LCST) and $D_{40°C}$ = 350–400 nm when above the LCST. **B.** Scanning Transmission Electron Microscopy (STEM) imaging of dry PNIPAM microgels. Scale bars: 5 μm. D_{Dry} = 350–400 nm. Scale bar: 500 nm. **C.** Cryo-Electron Microscopy (Cryo-EM) imaging of PNIPAM microgels snap-frozen in water below the LCST. The measured size of the PNIPAM via Cryo-EM was D_{RT} = 650–670 nm. Scale bar: 2 μm. **D.** Cryo-EM imaging of SiO_2@PNIPAM NPs snap-frozen in water below the LCST. The measured size of the SiO_2@PNIPAM NPs was D_{RT} = 480 ± 20 nm. The size of the SiO_2 cores was D_{Core} = 260 ± 10 nm and the thickness of the PNIPAM shell in swollen state was approximately T_{PNIPAM} = 100–120 nm. Scale bar: 1 μm. **E.** HAADF-STEM imaging of PNIPAM microgels dispersed in water. Spheres of around 400–450 nm in diameter where observed with inter-particle spacings of 650–700 nm. Dashed lines highlight one of such spheres. The size of these spheres corresponded to that of the unresponsive PNIPAM cores, and the inter-particle spacing corresponds to the total size of the microgels (core and corona). The observed particle size decreased in time under electron beam illumination,as shown in **F.**. Scale bars: 1 μm.

icon nitride window were imaged via (S) TEM and the size of the dry, collapsed microgels was D_{Dry} = 350–400 nm (Fig. 1B).

2.1.2. Cryo-EM: PNIPAM microgels and Silica-PNIPAM core–shell Particles

Cryo-EM is a powerful and well established method to image snap-frozen thin liquid layers inside an electron microscope [32,33]. Here we describe our cryo-EM measurements for our system of PNIPAM microgels (Fig. 1B) and as well a system of core–shell SiO_2@PNIPAM hybrid microgels (Fig. 1D). The measured size of the PNIPAM microgels in water below their LCST was D_{RT} = 650–670 nm is in accordance with the DLS measurements. Cryo-EM measurements of the SiO_2@PNIPAM NPs yielded a swollen total diameter for this system of D_{RT} = 460–500 nm. The size of the SiO_2 cores was D_{Core} = 260 ± 10 nm and therefore the thickness of the PNIPAM shell was in the range of T_{PNIPAM} = 100–120 nm. We report that attempts to snap-freeze PNIPAM microgels whilst in their collapsed state by starting from a dispersion at a temperature above the LCST were not successful, and their sizes below the LCST were observed.

2.1.3. LC-(S) TEM of PNIPAM microgels

LC-(S) TEM offers an excellent platform to study thin (up to a few microns) liquid samples with nanometric resolution [34]. Furthermore, the contents of these thin liquid layers can be precisely heated,[35] thus showing great potential to directly characterize *in situ* the thermoresponsive behavior of PNIPAM microgels and PNIPAM nanometric thin layers. However, LC-(S) TEM relies on the irradiation of a sample with an 80–300 keV electron beam, which can affect a sample directly and indirectly though the interaction of both the particles and solvent with beam-induced radiolysis products [36,24]. Here we characterize such electron beam induced effects on PNIPAM microgels in water and discuss the underlying chemistry.

PNIPAM microgels in water were imaged by means of Bright Field (BF) and High-Angle Annular Dark Field (HAADF) (S) TEM. A small volume of the suspension was drop-casted onto a glow discharged chip. Another glow discharged chip was placed on top of the solution and the cell was closed to create the liquid cell environment. Samples were loaded into a dedicated *in situ* liquid cell TEM holder. Upon imaging, PNIPAM particles gradually decreased in size while their contrast increased even at low electron doses of 4—20 $e^{-}nm^{-2}s^{-1}$ (Fig. 1E, F) which are already quite low as compared to 'ordinary' TEM imaging at these magnifications.The initial size of the visible PNIPAM part of the PNIPAM microgels visible in water corresponded to the previously defined $D_{40°C}$ (350–450 nm) of this system. Furthermore, the distance between the centers of the adjacent particles corresponded to values close to D_{RT} (650–700 nm), confirming that a corona with contrast so weak that it did not give a detectable signal was present around the visible

cores. This low contrast is consistent with the difficulties of detecting the corona with other scattering techniques (e.g.light scattering). Contrast in transmission electron microscopy depends critically on the elemental composition and density of a sample and increases with increasing electron dose rates and signal integration times. The volume occupied by the corona of PNIPAM microgels in water consists of a low volume fraction of polymer (< 10 vol.%) and thus it consists mostly of water [27]. Therefore, the generation of contrast for such structures in a swollen state in water relies on the use of relatively intense beams and sensitive detectors. However, our results show that PNIPAM microgels are additionally sensitive to radiolysis damage and therefore more intense beams are not a viable option, so that other strategies needed to be assessed. Use of low electron dose rates has been widely reported by our group and by others as critical to observe dynamic systems and chemically sensitive organic and inorganic particles [37–39]. Electron beam effects on the microgels during LC-(S) TEM experiments are discussed in more detail later in this article.

2.2. In situ characterization of thermoresponsive behavior of PNIPAM microgels and layers on core–shell particles

We have shown that volumes of a sample with low polymer volume fractions (<10 vol.%) are not easily resolvable in water via LC-EM at present state-of-the-art electron dose rate conditions. We therefore explored multiple strategies to generate contrast that allows the determination of the entire volume of the microgels, in particular two different approaches to achieve this end: altering the contrast of the solvent and labeling of the microgels. Results on dissolving Cu and U salts in the aqueous medium to increase solvent contrast, as well as on decorating PNIPAM microgels with a variety of Au (with a variety of capping ligands) and silicia based NPs are detailed in the Supplementary Information. In summary, electron beam irradiation resulted in the reduction of the metal ions into particles and coatings, preferentially on the PNIPAM microgels. Au NPs did not show efficient spontaneous attachment to the microgels, however silica NPs did. Core–shell Au@SiO_2 NPs with diameters of 17(core)@39(shell) ± 1@6 nm showed spontaneous attachment to PNIPAM microgels while still containing the highly scattering Au NP, and allowed for the direct imaging of the full size of the microgels in water. This labelling approach could also be adopted for the preparation of Cryo-EM samples. The ability to resolve the volume of the complete highly thermoresponsive PNIPAM coronas opens the door to directly observe PNIPAM's characteristic temperature induced phase transitions. To do so, microgel samples were prepared on liquid cell chips equipped with heating MEMS technology which enables increasing the temperature locally in the liquid cell volume (Variable Temperature LC-(S) TEM, or VT LC-(S) TEM). This allowed the *in situ* heating of the liquid cell volume, thereby inducing the microgel size transition when the LCST was crossed. **Fig. 2**A shows a swollen microgel below the LCST and a collapsed microgel above the LCST. Multiple thermoresponsive cycles where quantified by imaging at 20 °C and at 40 °C different areas of the liquid cell to avoid beam induced artifacts (Fig. 2B). Spectacularly, a large number of particles could be imaged per temperature set above or below the transition temperature, at nanometer resolution. As expected, this process was fully reversible.

The observed swollen and collapsed state of the PNIPAM micogels approximately matched with that measured via DLS and Cryo-EM (blue (RT) and red (40 °C) dashed lines). Interestingly, the measured size for the swollen state was slightly below the size measured by DLS and Cryo-EM, and the collapsed size was slightly above that for DLS. This could be an indication of the mechanism through which the Au@SiO_2 attached to the PNIPAM corona, with a given depth in the attachment to the swollen corona but with a hard limit when PNIPAM collapses and the SiO_2 acted as a spacer between the harder collapsed polymer shell and the high contrast Au core. An image of a dry sample of hard spherical NPs surrounded by Au@SiO_2 marker NPs where their silica shell can be seen acting as spacer between the high contrast cores and the "labelled" particle can be found in SI Fig. S3. A heating cycle was closely followed by increasing and decreasing in gradual steps the temperature of the cell around the LCST (Fig. 2C). The decrease in size of the microgels did not happen exactly around the *ex situ* LCST (shifted by about 2.5 °C to 30 °C). This shift could reflect changes in the LCST arising from the decoration of the microgels,[40] and/or errors emerging from *in situ* temperature control,[35,41] since the equilibrium temperature of the liquid volume depends on parameters such as sample thickness and/or flow speed. For completeness, we next evaluated the impact of electron beam irradiation of the microgels on their thermoresponsiveness (Fig. 2D). If cross-linking would be concurrently happening during our imaging, then a decrease in the ability to change in size upon heating would be expected. We found that 1 frame of very low dose electron beam (< 5 $e^{-}nm^{-2}s^{-1}$) irradiation affects the thermoresponsive capacity of PNIPAM microgels even in the presence of 2-propanol as radical scavenger. More precisely, the recovery of D_{RT} after heating above the LCST and imaging was hindered. A decrease of 100–150 nm of the total swollen size was observed across all samples after a single frame. This was independent on whether particles were fist imaged before (swollen) or after (collapsed) heating. If imaging was started at temperatures above the LCST and then the system was cooled down, the real D_{RT} of the microgel system could not be recovered even after hours after electron irradiation, confirming the permanent nature of the electron beam induced chemical changes in their polymeric structure. This follows also from our observations that a similar degree of shrinkage was observed for all electron doses even in the presence of radical scavengers reported in the previous sections.

We then extended the same procedure to SiO_2@PNIPAM NPs (Fig. 2E). The thin PNIPAM shell was indeed clearly observed from the positions of the marker NPs with respect to the core surface. Furthermore, above the LCST we also observed the reversible shrinkage of the thin PNIPAM layers to thicknesses down to 50–60 nm (Fig. 2F). Again the measured size for the most swollen state was slightly lower than the size measured via Cryo-EM. In summary, we demonstrate that the thermoresponsive behavior of PNIPAM microgels and PNIPAM shell layers grafted onto hard core-particles can be easily studied in the VT LC-(S) TEM set-up with the use of high contrast marker NPs with nanometric resolution. This possibility opens the door to directly characterize the temperature evolution of PNIPAM systems (sub-100 nm microgels and coatings) with thicknesses and geometries not measurable with DLS or other conventional techniques [42]. It is worthwhile mentioning that although hysteresis of the thermoresponsive behavior of PNIPAM has been reported in the literature, we do not detect it in our measurements. Since our method images the microgels once they reach a stable state at each temperature, as limited by electron-beam induced radiolysis effects,[43] it is possible that our system presents hysteresis effects we still cannot detect.

2.3. In situ characterization of PNIPAM co-nonsolvency in aqueous alcoholic solvents

The microfluidic capabilities of dedicated liquid cell holders allow changing *in situ* the solvent present in the liquid cell. We exploited this to directly characterize solvent-induced phase transitions. All samples were prepared as described previously by loading them with ultrapure water. Assembling the cell with alcoholic solutions is difficult due to the fast evaporation rates of alcohols, as

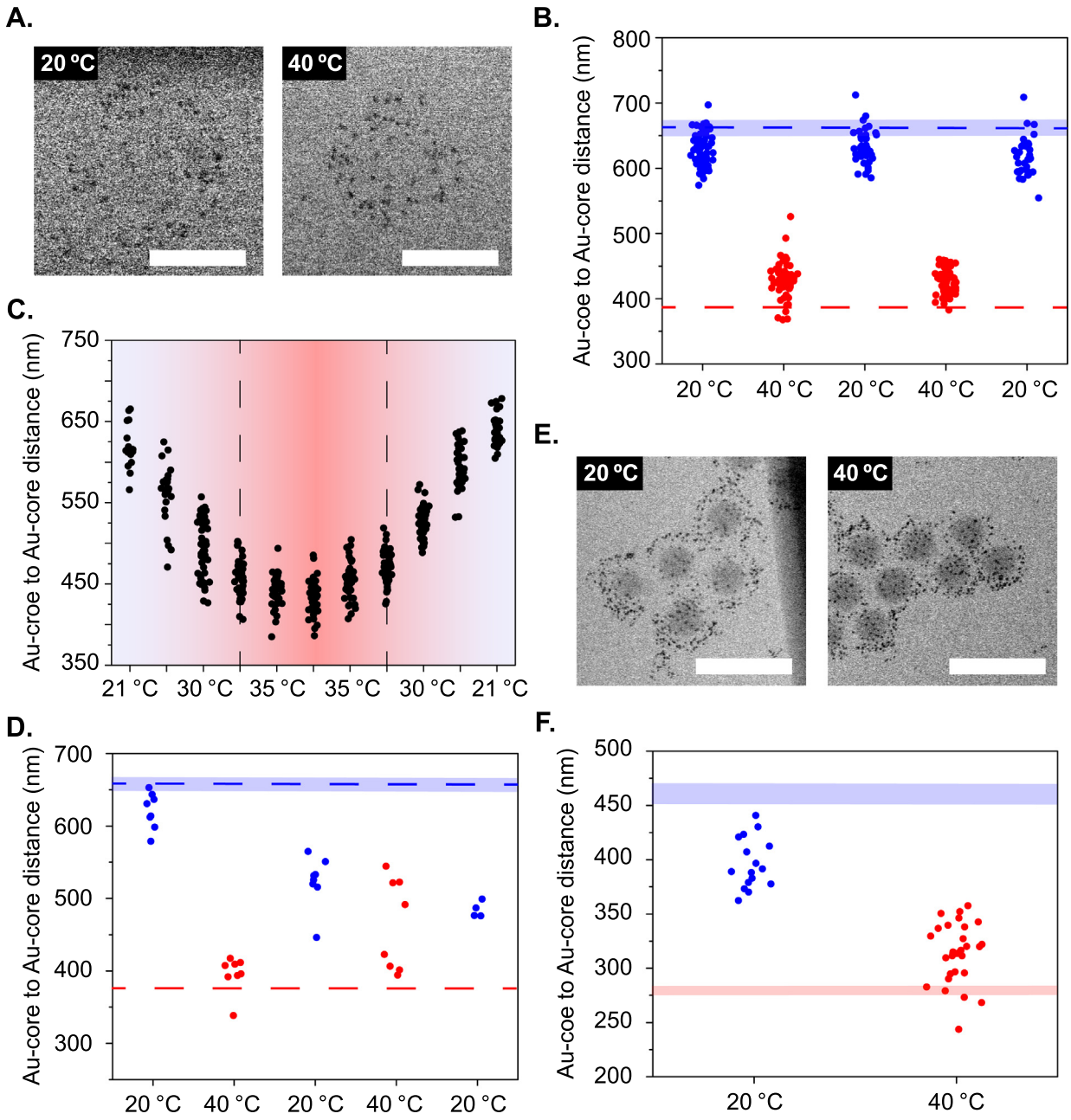

Fig. 2. *In situ* **characterization of the thermoresponsive behavior of PNIPAM microgels and core–shell with nanometric resolution A.** BF-(S) TEM imaging of two different PNIPAM micogels below (at 20 °C) and above (at 40 °C) the LCST. Scale bars: 400 nm. **B.** Measurements for the sizes of multiple microgels during multiple heating–cooling cycles. For each temperature different regions were imaged to avoid beam induced artifacts. Dashed lines indicate the sizes measured via DLS for our system below (blue) and above (red) the LCST. The blue horizontal bar indicates the size as measured via Cryo-EM. **C.** Detailed size evolution of PNIPAM microgels during a heating cycle. Particle size started decreasing prior arriving to the LCST, potentially reflecting slight deviations between the expected and the real temperature of the liquid volume. **D.** Size evolution of the a set of PNIPAM microgels over two heating–cooling cycles imaged at low electron dose rates ($<5\ e^{-}nm^{-2}s^{-1}$). The same microgels were imaged at each temperature. The full size of the particles below the LCST could not be recovered and the thermoresponsive capacity was damped. **E.** BF-(S) TEM imaging of two different SiO_2@PNIPAM microgels below (at 20 °C) and above (at 40 °C) the LCST. Scale bars: 750 nm. **F.** Measurements for the sizes of multiple core–shell SiO_2@PNIPAM NPs during multiple heating–cooling cycles. For each temperature different regions were imaged to avoid beam induced artifacts. The blue and red horizontal bars indicate the swollen size measured via Cryo-EM for our system below the LCST (blue) and the size of the bare SiO_2 core measured via TEM. (For interpretation of the references to colour in this figure legend, the reader is referred to the web version of this article.)

microliter droplets are dropcasted and the evaporation time can be close to the cell assembly time. Therefore, loading the cells with water and introducing the alcoholic solutions via microfluidics was the most reliable method. To ensure that the local solvent composition at the liquid cell windows was that of the intended solvent, all solvent mixtures were premixed prior to flowing them into the cell, and solvent flow was maintained for at least 30 min prior to imaging. We characterized PNIPAM's co-nonsolvency in methanol/water mixtures (Fig. 3A). The co-nonsolvency effect is the collapse of PNIPAM microgels in this mixture,[10,11] while in pure methanol and water the microgel is in a swollen state. To ensure that the local solvent composition at the liquid cell windows was that of the intended solvent, all solvent mixtures were premixed prior flowing them into the cell and solvent flow was maintained for at least 30 min prior to imaging. A phase transition from the regular swollen state in water was observed in a mixture

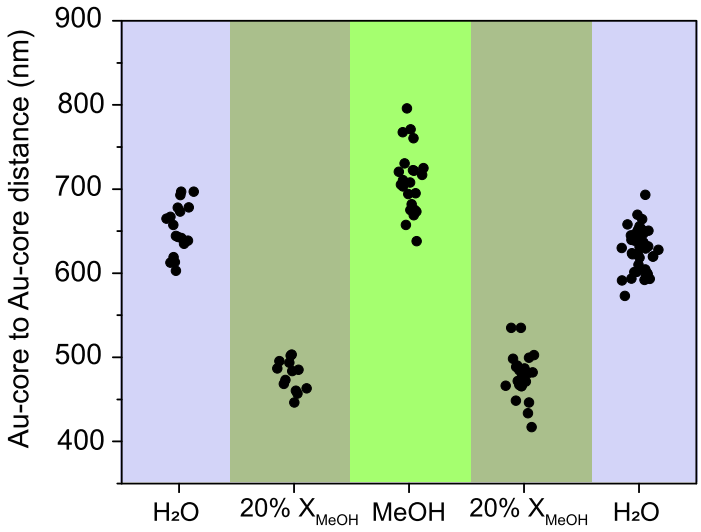

Fig. 3. *In situ* **characterization of the co-nonsolvency in aqueous alcoholic solvents of PNIPAM microgels with nanometric resolution. A.** Measured microgel sizes in pure water, a methanol/water mixture (20% molar ratio of methanol) and in methanol. In the methanol/water solvent e articles underwent a phase transition to a collapsed state comparable to that for heating in water above the LCST. Microgels were swollen in water and in methanol, and particle sizes measured in methanol were slightly larger than in water.

of 20% molar ratio of methanol comparable to that observed upon heating above the LCST. When the solvent was replaced with just methanol, we observed swollen microgels with slightly bigger particle sizes than that in water. This process was then reversed by going back to the methanol/water mixture and then pure water, for which similar size distributions were measured. These results are in agreement with measurements of this phenomenon using other techniques [10].

2.4. LC-(S) TEM imaging of PNIPAM: Radiolysis damage

We showed that the unobserved size of PNIPAM microgels in water decreases under electron beam illumination. This decrease in size was correlated with the intensity of the electron beam (Fig. 4A), with higher electron beam dose rates resulting in a faster shrinking. By performing "post-mortem" analysis of the samples after opening the liquid cell (Fig. 4B) we confirmed that the particles that resulted from electron irradiation in water showed after drying a smaller diameter and an enhanced contrast corresponding to higher density particles. We then confirmed that this high contrast portion of PNIPAM microgels in water corresponded to the relatively thermally unresponsive cores. By means of *in situ heating LC-(S) TEM we checked that the observable size of the PNIPAM microgels did not depend on whether the temperature of the system was below or above the LCST (Fig. 4C). Furthermore, the shrinkage behavior was reproducible and the same for all temperatures. The extent of local beam-induced temperature changes in liquid cell experiments has been recently debated in literature, although it appears to be limited to a few degrees after some minutes of continuous irradiation for low electron dose rates [44,45]. As the beam effects that we observed did not differ between absolute changes of temperature above tens of degrees, we believe that electron beam damage in water on polymers is not a result of, nor is dependant on, beam induced local temperature changes.*

In order to understand the reported shrinkage behavior of our PNIPAM microgels, the chemical and physical processes that happen during (S) TEM imaging of a polymeric chain in water have to be considered. The irradiation of water by a (S) TEM electron beam is known to generate a number of radiolysis products [36,24]. Of such species, two are of most interest in this study: hydroxyl radicals ($OH^{\cdot}$) and hydrogen radicals ($H^{\cdot}$). These radicals react strongly with polymeric chains via hydrogen atom abstraction, which results in the transformation of the polymer chains into macroradicals. Concurrently, the electron beam can also directly generate polymer macroradicals. Such macroradicals can react with each other forming cross-linked structures, in a process named inter-molecular recombination (cross-linking between different polymeric chains) or intra-molecular recombination (cross-linking between parts of the same polymeric chain), among other reactions [47–49,46]. A schematic of the proposed mechanism behind the shrinkage of PNIPAM microgels upon electron beam illumination in a liquid cell can be seen in Fig. 4D. Intramolecular cross-linking has been shown to reduce the radius of gyration of a number of polymers (e.g. poly(vinyl alcohol), poly(vinyl pyrrolidone) or poly(acrylic acid)) [47–49]. This process would result in more condensed and cross-linked, smaller PNIPAM particles.

2.5. Increasing microgel stability with radical scavengers

The impact of radiolysis products in LC-(S) TEM experiments has been addressed with varying success by scavenging such species. This is achieved by changing the chemical composition of the liquid media introducing radical scavengers, i.e. molecules that react with radicals more efficiently than the system of interest. This results in a less harsh environment for the polymer, as the main radiolytic species are partially removed from the system by the scavengers. This strategy has been widely used in LC-EM studies, and can be readily adapted to our system. [24] Hydroxyl radicals ($OH^{\cdot}$) and hydrogen radicals ($H^{\cdot}$) can be scavenged by the presence of alcohols in solution, with isopropanol (ISO) being an effective radical scavenger. Hydrated electrons ($e^{-}_{(aq)}$) can also be scavenged by adding acetones in solution. The reaction of such scavengers with these relevant water radiolysis radicals results in products with lower redox potential and therefore reduces the harshness of the aqueous media to the PNIPAM microgels (**Fig. 5**A) [50,51,24]. Poly(diethylene glycol methyl ether methacrylate) (PDEGMA)-based block copolymers dispersed in aqueous medium have been shown to survive higher electron dose rates

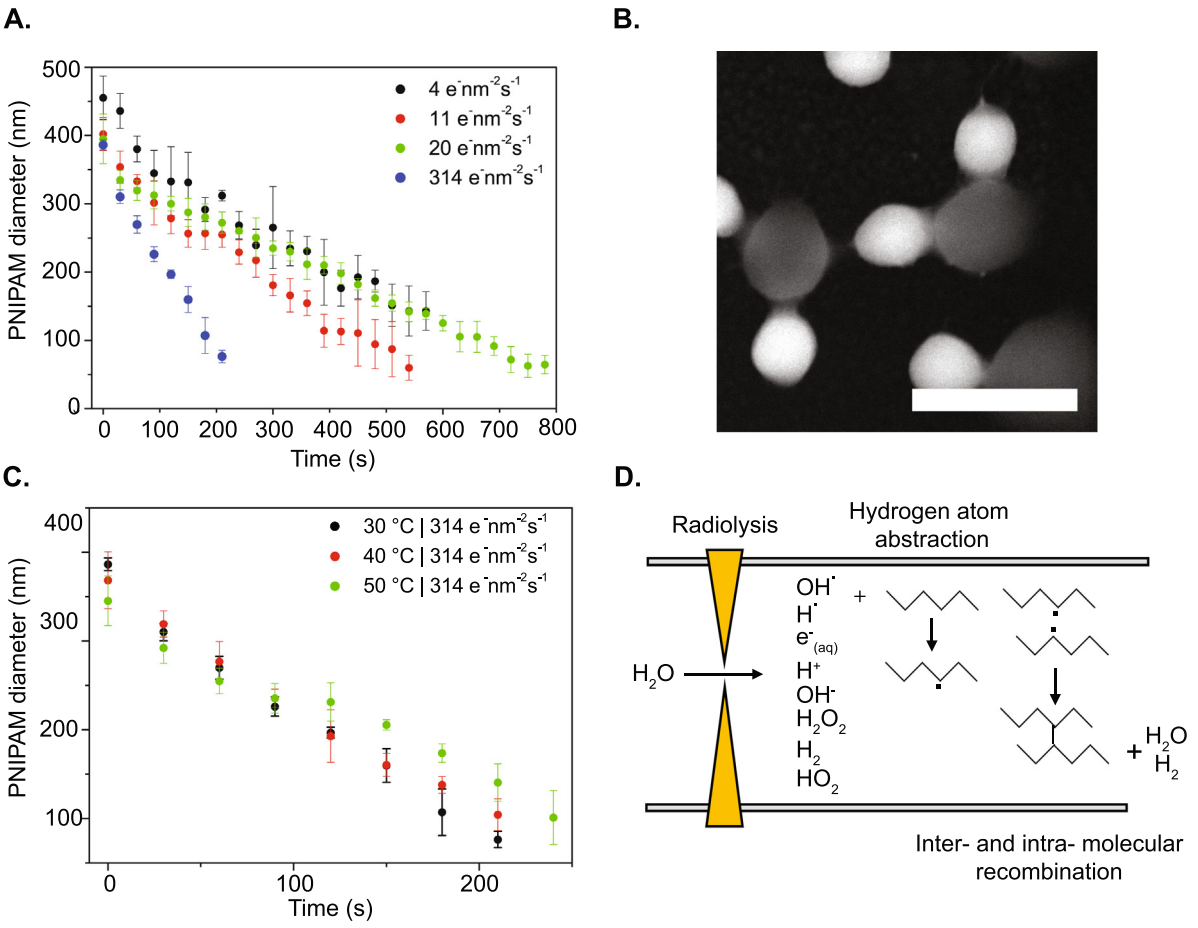

Fig. 4. Characterization of electron beam effects on PNIPAM microgels in water. A. *Decrease of measured PNIPAM size in time for a number of electron dose rates at 20 °C. Low electron dose rates (4–20 $e^{-}nm^{-2}s^{-1}$) resulted in slower shrinkage compared to a medium electron dose rate (314 $e^{-}nm^{-2}s^{-1}$).* **B.** *Post-mortem LC-(S) TEM sample of an irradiated area showing both irradiated and unirradiated, dried particles. Small, high-contrast particles correspond to the irradiated microgels. Big, low-contrast particles correspond to PNIPAM microgels that diffused and dried on this region during the disassembly of the liquid cell. Scale bar: 700 nm.* **C.** *Decrease of measured PNIPAM size in time for an electron dose rate of 314 $e^{-}nm^{-2}s^{-1}$ at higher temperatures (around and above the LCST). The initial observed size of the microgels did not change, confirming the unresponsive nature of the polymer dense PNIPAM core.* **D.** *Interplay between chemistry of water radiolysis due to electron beam illumination and chemistry of polymers and water radicals [24,46].*

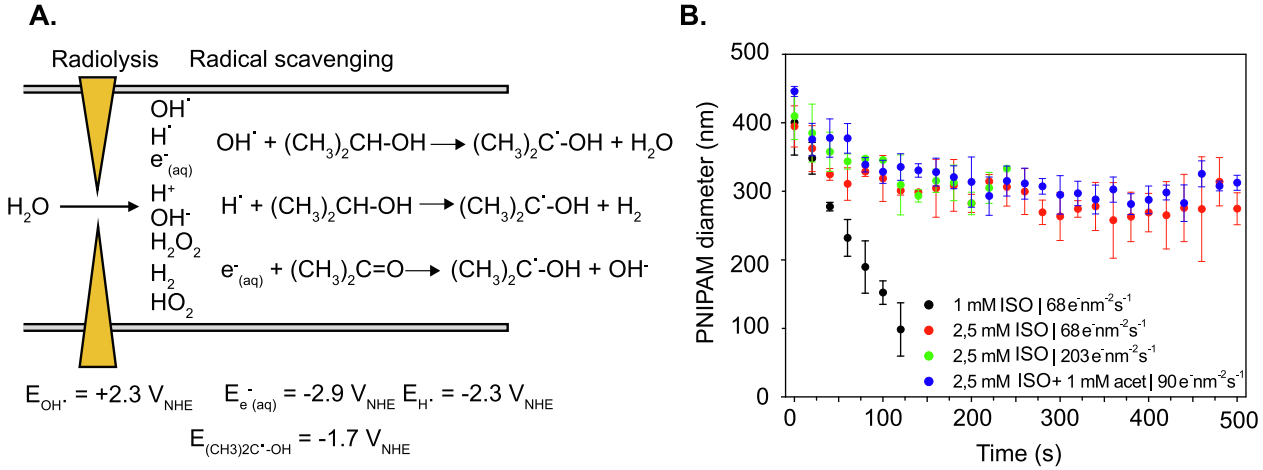

Fig. 5. Increasing PNIPAM microgel stability under electron beam illumination in water with radical scavengers A. Chemistry describing the scavenging of H·, OH·, $e^{-}_{(aq)}$ by isopropanol (ISO) and acetone. The resulting product of the reaction between the radicals and the scavengers have less reactive redox potentials. **B.** The addition of ISO partially stabilized the shrinking of PNIPAM microgels after an initial shrinkage of around 20% of the particle size. A minimal concentration of 5 mM ISO was needed to scavenge enough radicals for this effect to be substantial at a low electron dose of 28 $e^{-}nm^{-2}s^{-1}$. This relative stability was maintained even at medium electron dose rates of 203 $e^{-}nm^{-2}s^{-1}$. The addition of small amounts of acetone to scavenge hydrated electrons did not result in further stability improvements.

in liquid phase EM experiments in the presence of isopropanol [52].

We imaged PNIPAM microgels in the presence of various radical scavengers to assess their impact on PNIPAM stability during liquid phase EM experiments (Fig. 5B) as compared to pure water. PNIPAM stability in water under electron irradiation increased for concentrations of ISO above 2.5 mM for doses as high as 203 $e^{-}nm^{-2}s^{-1}$. The presence of acetone (1–5 mM), scavenging $e^{-}_{(aq)}$, did not result in stability improvements. Although an initial shrinkage phase of around 20% of the particle diameter still happened for all media, the shrinkage stopped and did not proceed as was observed for PNIPAM colloids in pure water. Interestingly, the ability to image PNIPAM colloids at higher electron dose rates ($>$ 500 $e^{-}nm^{-2}s^{-1}$) resulted in the observation of an anisotropic shrinkage/dissolution of the colloids, with higher shrinkage/dissolution rates in the direction perpendicular to the scanning direction of the electron beam and/or deformation of the particle towards an ellipsoidal shape with the long axis in the scanning direction (Supplementary Fig. S6). Similar anisotropic and/or deformation of the particle towards an ellipsoidal shape with the long axis in the scanning direction have been previously reported for silica particles dispersed in water and water/ethanol/ammonia mixtures in LC-EM experiments and it is interesting for future studies to investigate if these electron beam-induced deformations for totally different types of particles are related [53,39].

3. Conclusions

In this study we report the successful single particle characterization of thermally and co-nonsolvency induced phase transitions of PNIPAM microgels and PNIPAM shells *in situ in water via liquid phase electron microsopy. We show that the ability to resolve a solvated polymeric volume from its surrounding media in EM depends critically on the polymer volume fraction, which makes imaging at realistic, presently state-of-the-art dose impossible. We demonstrate that this limitation can be overcome by labelling the PNIPAM structures via an in situ post-synthetical labelling step with high contrast core–shell silica@Au NPs. Silica-based NPs spontaneously attach predominantly on the outside of PNIPAM corona's, simplifying the labelling step. The ease to resolve these NPs even when immersed in liquid allows us to image and measure the size of PNIPAM microgels and shells at different temperatures and in different solvents with nanometer resolution. Temperature and solvent composition were controlled and changed in situ using microfluidics, in contrast with measurements from other electron microscopy techniques such as cryo-EM [18,19].*

In order to arrive at a labelling technique that worked, the implications of using electron irradiation to image PNIPAM in water were also explored experimentally. We show that PNIPAM microgels shrink irreversibly upon electron beam illumination and that this process is mediated via water radiolysis radicals. Scavenging such species with isopropanol partially protects the microgels but not completely, and some degree of shrinkage was unavoidable, while in addition alcohols have a co-nonsolvency effect on PNIPAM in water and thus modify the thermoresponsive behavior. We found as well that PNIPAM microgels are a good substrate for the reduction of metal ions into NPs and coatings. Electron beam induced incorporation of ligand-capped Au NPs onto the microgels was observed for citrate and PEG (with and without additional chemical functionalizations) capped Au NPs. Au NPs capped with acid-functionalized PEG molecules formed branched structures under electron beam illumination, both on the imaging windows and onto the surface of the microgels. Electron beam effects are thus the main limitation preventing our method to more continuously follow PNIPAM's thermoresponsive behavior. The incorporation to our methodology into state-of-the-art microscopy developments aimed at reducing the number of electrons required to acquire an EM image, such as the use of direct electron detectors and sparse scanning methods, may overcome such constraints.

4. Methods

4.1. Materials

N-isopropylacrylamide (NIPAM, 99 %, Sigma–Aldrich), N,N'-methylenebis- acrylamide (BIS, 99 %, Sigma–Aldrich), Ultrpure water (milliQ grade, Millipore system), Potasium Persulfate (KPS, 99%, Sigma–Aldrich), Tetraethyl Orthosilicate (TEOS, 99%, Sigma–Aldrich), 3-(Trimethoxysilyl) propyl meth- acrylate (TPM, 98%, Merck) L-arginine (98%, Sigma–Aldrich), Potasium Hydroxide (KOH, reagent grade, $\geqslant$98%, pellets, Sigma–Aldrich), Hydrogen Tetrachloroaurate Trihydrate ($HAuCl_4 \cdot 3H_2O$, $\geqslant$99.9%, Sigma–Aldrich), Sodium Citrate Tribasic Dihydrate ($\geqslant$99.0%, Sigma–Aldrich), Sodium Hydroxide (NaOH, $\geqslant$97.0%), α-Mercapto-ω-Mercapto Polyethylene Glycol (MW 5 kDa, H_3CO-PEG-SH,Rapp Polymere), α-Mercapto-ω-Amino Polyethylene Glycol Hydrochloride (MW 5 kDa, HS-PEG-NH_2·HCl, Rapp Polymere) and α-Mercapto-ω-Carboxy Polyethylene Glycol (MW 5 kDa, HS-PEG-COOH, Rapp Polymere).

4.2. Synthesis of PNIPAM microgels and SiO_2@PNIPAM NPs

PNIPAM microgels were synthesized by radical emulsion polymerization. 10 mg of NIPAM and 1.0 mg of BIS were dissolved in 710.0 g of water. This solution was then sealed and bubbled with nitrogen to remove dissolved oxigen. Bubbling was then stopped and the flask was placed in a oil bath at 70 °C. When the solution reached 70 °C a solution of 10 mg of KPS in 10.0 mL of water was quickly injected to start the radical polymerization process. This reaction was left to continue at 70 °C for 4 h while stirring. The final product was cleaned by letting the solution to cool down, centrifugation and redispersion in water. SiO_2@PNIPAM NPs were synthesized via the same radical emulsion polymerization method but in the presence of TPM coated Stöber silica [54].

4.3. Synthesis of amino acid catalyzed (AAC) silica NPs

AAC Silica particles (113 nm diameter, polydispersity: 3%, from TEM imaging) were synthesized with a three step synthesis based on previous literature [55]. All glass work was etched of residual silica of former silica synthesis via a base bath (2–3 days in a saturated solution of KOH in ethanol, rinsed with milliQ water). First, 28 nm cores were synthesized as follows: in a 500 mL 1-neck flask 182.5 mg (6 mM) L-arginine was dissolved in 169 mL milliQ water. The mixture was heated to 70 °C and stirred slowly (200 rpm). After 1 h, 11.2 mL (49 mmol) of TEOS was added slowly via the wall. The reaction mixture was stirred for 1 day to complete the synthesis. These cores were overgrown up to a diameter of 55 nm as follows: in a 500 mL 1-neck flask (base bath, KOH in ethanol) 183.5 mg (6 mM) L-arginine was dissolved in 169 mL milliQ water. 19.3 mL of the dispersion of 28 nm silica particles was added. The mixture was heated to 70 °C and stirred slowly (200 rpm). After 1 h, 11.2 mL (49 mmol) of TEOS was added slowly via the wall. The reaction mixture was stirred for 1 day to complete the synthesis. These nanoparticles were overgrown up to the final 113 nm diameter as follows: in a 500 mL 1-neck flask (base bath, KOH in ethanol) 182 mg (0.006 M) L-arginine was dissolved in 169 mL milliQ water. 19.3 mL of the dispersion of 55 nm silica particles was added. The mixture was heated to 70 °C and stirred slowly (200 rpm). After 1 h, 11.2 mL (49 mmol) of TEOS was added

slowly via the wall. The reaction mixture was stirred for 1 day to complete the synthesis.

4.4. Synthesis of citrate stabilized and PEG-capped gold nanoparticles (AuNPs)

4.4.1. Synthesis of AuNPs

Citrate stabilized spherical AuNPs were synthesised using the sodium citrate reduction method1,2: 100 mL water and 1.00 mL of an aqueous solution containing 10.0 g/L $HAuCl_4 \cdot 3\ H_2O$ were added to a 250 mL two-neck flask with stirring bar and reflux condenser. The flask was placed in an oil bath and heated until boiling. Then, 3.0 mL of an aqueous solution containing 10.0 g/L sodium citrate tribasic dihydrate was rapidly added under vigorous stirring (1200 rpm) and the mixture was left refluxing and stirring for 15 min during which a colour change from yellow to dark blue to pink and finally deep red was observed. Stirring was slowed down to 400 rpm, the oil bath was removed and the mixture was allowed to cool down to room temperature. The resulting AuNPs had a mean diameter of 16.7 nm with a polydispersity of 1.1 nm (6.3%) based on TEM imaging.

4.4.2. PEGylation of AuNPs

The AuNPs were functionalized by covalently binding thiolated polyethylene glycol (PEG) ligands to the AuNP surface. To 10.0 mL of the as synthesized AuNP dispersion 0.50 mL of an aqueous 10.0 g/L solution (2 mM) of one of the PEG ligands (H_3CO-PEG-SH, HS-PEG-NH_2·HCl or HS-PEG-COOH) was added, followed by 0.25 mL of a 0.10 M aqueous NaOH solution. The ligand concentration corresponded to 50 PEG molecules per nm^2 of gold surface. The reaction was left to proceed for at least 1 h, but the solution could be stored without further purification for $\geqslant$2 years. To concentrate the particles and remove unreacted ligands prior to further use, the particles were washed using centrifugation (15000 RCF for 30 min in 5 mL Eppendorf centrifugation tubes) and redispersion of the sediment in 10.0 mL of water, followed by another round of centrifugation and redispersion of the sediment in 0.50 mL of water.

4.4.3. Coating of Au core NPs with a SiO_2 shell

A silica shell was grown around the AuNP seeds using a PVP-mediated Stöber shell growth:[56,57] 720 μL of a 0.10 g/mL solution of PVP in water was added to 30 mL of the AuNPs and stirred (300 rpm) for 24 h. The PVP-coated particles were collected by means of centrifugation (15000 g, 20 min. in 5 mL Eppendorf tubes), redispersed in 30 mL ethanol and added to a 40 mL glass vial, and stirred at 1200 rpm. Then, 3.00 mL ammonium hydroxide solution was added, followed by 50.0 μL of a freshly prepared 10% vol. TEOS in ethanol. After 5 min, the stirring speed was reduced to 400 rpm and the mixture was left to react for 4 h. The resulting AuNP@SiO_2 particles had a total diameter of 39 nm with a polydispersity of 6 nm. The particle dispersion could be stored at room temperature without further purification for at least 1 year prior to use.

4.5. Cryo- Electron Microscopy (Cryo-EM)

Samples were prepared in cryo-EM dedicated grids with a Thermo-Fischer Scientific Vitrobot. Blotting time was 1 s and snap dipped in liquid ethane. Samples were kept in liquid nitrogen at all times after preparation. Samples were loaded in a Gatan cryo holder and images by a Thermo-Fisher Scientific Tecnai 20 transmission electron microscope equipped with a field emission gun operating at 200 kV.

4.6. Liquid cell transmission electron microscopy

Liquid Cell Scanning EM samples were loaded in a dedicated liquid cell holder (Protochips, Poseidon Select) equipped with flow and *in situ heating capabilities. The spacer size was of 500 or 1000 nm in all experiments with PNIPAM microgels and 150 nm for all experiments with hybrid silica@PNIPAM microgels. To make sure that the particles were in pure water, samples were subjected to a flow of ultrapure water (1 μl/min) for at least 3 h. Frames were acquired at 1024x1024 pixels, 3 nm pixel size, 28 μs dwell time. All experiments were repeated at least 3 times.*

Sample preparation

The top and bottom silicon chips were glow discharged for 1 min to ensure the wettability of the chips. Then, 2 μl dilute dispersion of $\sim$ 10 mg/L of the desired microgels in water was drop-casted on the top chip and was allowed to dry almost completely. When the sample was almost dry, the bottom chip was loaded on the holder tip and 2 μl of water or a aqueous dispersion of NPs were drop-casted on it and the sample was sealed with the top chip (containing the microgels). Bottom chips with gold spacers of 150 for SiO_2@PNIPAM NPs and of 500 and 1000 nm for PNIPAM microgels. This sample preparation procedure ensured high microgel coverage of the liquid cell imaging window and as well a minimal liquid thickness.

Imaging

TEM and (S) TEM imaging were performed with a Thermo-Fisher Scientific Talos F200X transmission electron microscope equipped with a field emission gun operated at 200 kV. High angle annular dark field (HAADF) STEM imaging was performed with camera lengths of 120 mm for dry samples and from 120 to 220 mm for liquid samples, as depending on the liquid layer thickness resulting from sample preparation different camera lengths gave the best contrast. Beam currents were measured though the fluorescent screen current in vacuum and are reported in the main text.

The electron dose rate was calculated as follows: [58]

$$d = \frac{I_e}{eA} \tag{1}$$

Where d is the electron dose rate, I_e is the beam current, e is the elementary charge, and A is the total frame size determined by the magnification.

4.7. Dynamic light scattering

Particle sizes were measured by a home build dynamic light scattering (DLS) setup. A glass cuvette filled with a dispersion of the particles was suspended in a toluene bath. The toluene bath was thermostated using a Haake DC50 water bath. The sample was illuminated with a 632.8 nm He laser (30 mW) and the scattered light was collected by two optical fibers. Light was detected with a single photon detector (PMT-120-OP, S/N: 14962). A digital correlator (Flex01-12D) was used to cross-correlate the detected signals from both both collected signals. The data was analyzed using the cumulant method and particle diameter was calculated using the Stokes–Einstein relation (which should be considered an approximation for microgels, given the diffused nature of the microgel surface).

Author contributions

A. Grau-Carbonell performed Cryo-EM and LC-(S) TEM experiments. F. Hagemans synthesized PNIPAM microgels and performed DLS measurements. N. Elbers synthesized the silica-PNIPAM hybrid microgels. M. Bransen synthesized Au based NPs. R.J.A. van Dijk-Moes synthesized silica NPs. S. Sadighikia and T.A.J. Welling assisted in LC-(S) TEM experiments. A.van Blaaderen and M.A. van Huis supervised and initiated this research.

Declaration of Competing Interest

The authors declare that they have no known competing financial interests or personal relationships that could have appeared to influence the work reported in this paper.

Acknowledgements

This project received funding from the European Research Council (ERC) via the ERC Consolidator Grant NANO-INSITU (Grant No. 683076). F. Hagemans was funded by the Netherlands Organisation for Scientific Research (NWO). N. Elbers was supported by the Industrial Partnership Programme (IPP) Innovatie Physics for Oil and Gas (iPOG) of the 'Stichting voor Fundamenteel Onderzoek der Materie' (FOM), which was supported financially by Nederlandse Organisatie voor Wetenschappelijk Onderzoek (NWO). The IPP iPOG is cofinanced by Stichting Shell Research.. The authors also acknowledge funding from the NWO-TTW Perspectief Program "Understanding Processes Using Operando Nanoscopy," project UPON-B3 (No. 14206). M.B. acknowledge funding from the Netherlands Center for Multiscale Catalytic Energy Conversion (MCEC), an NWO Gravitation programme funded by the Ministry of Education, Culture, and Science of the government of the Netherlands.

Appendix A. Supplementary material

Supplementary data associated with this article can be found, in the online version, at https://doi.org/10.1016/j.jcis.2022.12.116.

References

[1] Y. Guan, Y. Zhang, Soft Matt. 7 (14) (2011) 6375.
[2] H. Kawaguchi, Polym. Int. 63 (6) (2019) 925.
[3] Z. Farooqi, S. Khan, R. Begum, Mater. Sci. Technol. 33 (2) (2016) 129.
[4] D. Roy, W. Brooks, S. Sumerlin, Chem. Soc. Rev 42 (17) (2013) 7214.
[5] A. Choe, J. Yeom, R. Shanker, M. Kim, S. Kang, K. Hyunhyub, NPG Asia Mater. 10 (2018) 912.
[6] J. Scarpa, D. Mueller, I. Klotz, J. Am. Chem. Soc. 89 (24) (1967) 6024.
[7] H. Schild, Prog. Polym. Sci. 17 (2) (1992) 163.
[8] S. Fujishige, K. Kubota, I. Ando, J. Phys. Chem. 93 (8) (1989) 3311.
[9] S. Carregal-Romero, N. Buurma, J. Perez-Juste, L. Liz-Marzán, P. Hervés, Chem. Mater. 22 (10) (2010) 3051.
[10] C. Scherzinger, A. Schwarz, A. Bardow, K. Leonhard, W. Richtering, Curr. Opin. Colloid. Interface. Sci. 19 (2) (2014) 84.
[11] H. Pérez-Ramírez, C. Haro-Perez, G. Odriozola, A.C.S. Appl, Polym. Mater. 1 (11) (2019) 2961.
[12] F. Scheffold, Nat. Commun. 11 (2020) 4315.
[13] M. Reufer, P. Díaz-Leyva, I. Lynch, F. Scheffold, Eur. Phys. J. E 28 (2009) 165.
[14] S. Höfl, L. Zitzler, T. Hellweg, S. Heminghaus, F. Mugele, Polymer 48 (1) (2007) 245.
[15] A. Alsayed, M. Islam, J. Zhang, P. Collings, A. Yodh, Science 309 (5738) (2005) 1207.
[16] Y. Peng, Z. Wang, A. Alsayed, A. Yodh, Y. Han, Phys. Rev. Lett. 104 (20) (2010) 205703.
[17] M. Gaurasundar, S. Nöjd, M. Braibanti, P. Schurtenberger, F. Scheffold, Colloids Surf. A: Physicochem. Eng. Asp. 499 (2016) 18.
[18] J. Crassous, B. Matthias, N. Drechsler, J. Schmidt, Y. Talmon, Langmuir 22 (6) (2006) 2403.
[19] J. Crassous, N. Rochette, M. Wittemann, M. Schrinner, M. Ballauff, M. Drechsler, Langmuir 25 (14) (2009) 7862.
[20] E. Ring, N. de Jonge, Microsc. Microanal. 16 (1) (2010) 622.
[21] N. Hodnik, G. Dehm, K. Mayrhofer, Acc. Chem. Res. 49 (9) (2016) 2015–2022.
[22] J. van Omme, H. Wu, H. Sun, A. Beker, M. Lemang, R. Spruit, S. Maddala, A. Rakowski, H. Friedrich, J. Patterson, H. Pérez Garza, J. Mater. Chem. C. 8 (31) (2020) 10781.
[23] H. Demers, N. Poirier-Demers, D. Drouin, N. de Jonge, Microsc. Microanal. 16 (2010) 795.
[24] T.J. Woehl, P. Abellan, J. Microsc. 265 (2) (2017) 135.
[25] A. Gelissen, A. Oppermann, T. Caumanns, P. Hebbeker, S. Turnhoff, R. Tiwari, S. Eisold, Y. Lu, J. Mayer, W. Richtering, A. Walther, D. Wöll, Nano Lett. 16 (22) (2016) 7295.
[26] X. Wu, R. Pelton, D. Hamielec, W. McPhee, Colloid. Polym. Sci. 272 (1994) 467.
[27] A. Mourran, Y. Wu, R. Gumerov, A. Rudov, I. Potemkin, A. Pich, M. Möller, Langmuir 32 (23) (2015) 723.
[28] A. Karanastasis, Y. Zhang, G. Kenath, M. Lessard, J. Bewersdorf, C. Ullal, Mater. Horiz. 5 (2018) 1130.
[29] M. Kwok, Z. Li, T. Ngai, Langmuir 29 (30) (2013) 9581.
[30] G.M. Conley, S. Nöjd, M. Braibanti, P. Schurtenberger, F. Scheffold, Colloids Surf., A Physicochem. Eng. Asp. 2016, 499 18.
[31] E. Siemes, O. Nevskyi, D. Sysoiev, S. Turnhoff, A. Oppermann, T. Huhn, W. Richtering, D. Wöll, Angew. Chemie - Int. Ed. 57 (38) (2018) 12280.
[32] R. Williams, D. McComb, S. Subramaniam, MRS Bull. 44 (12) (2019) 929.
[33] X. Benjin, L. Ling, Protein Sci. 29 (4) (2020) 872–882.
[34] S. Pu, C. Gong, A. Robertson, R. Soc, Open Sci. 7 (2020) 191204.
[35] T. van Swieten, T. van Omme, D. van den Heuvel, S. Vonk, R. Spuit, F. Meirer, H. Perez Garza, B. Weckhuysen, A. Meijerink, F. Rabouw, R. Geitenbeek, A.C.S. Appl, Nano Mater 4 (4) (2021) 4208.
[36] N.M. Schneider, M.M. Norton, B.J. Mendel, J.M. Grogan, F.M. Ross, H.H. Bau, J. Phys. Chem. C 118 (2014) 22373.
[37] L. Parent, V. Vratsanos, B. Jin, J. De Yoreo, N. van Gianeschi, MRS Bull. 45 (2020) 727.
[38] T. Welling, S. Sadighikia, K. Watanabe, A. Grau-Carbonell, M. Bransen, D. Nagao, A. van Blaaderen, M. van Huis, Part. Part. Syst. Charact. 37 (6) (2020) 2070014.
[39] A. Grau-Carbonell, S. Sadighikia, T. Welling, R. van Dijk-Moes, R. Kotni, M. Bransen, A. van Blaaderen, M. van Huis, A.C.S. Appl, NanoMater. 4 (2) (2021) 1136.
[40] S.-K. Lee, Y. Park, K. Jongseong, Appl. Sci. 8 (10) (2018) 1984.
[41] B. Fritsch, A. Hutzler, M. Wu, S. Khadivinazar, L. Vogl, M. Jank, M. Marz, E. Spiecker, Nanoscale Adv. 3 (2021) 2466–2474.
[42] J. Schmitt, C. Hartwig, J. Crassous, A. Mihut, P. Schurtenberger, V. Alfredsson, RSC Adv. 10 (2020) 25393.
[43] L. Blackman, D. Wright, M. Robin, M. Gibson, R. O'Reilly, ACS Macro Lett. 4 (11) (2015) 1210.
[44] H. Zheng, S. Claidge, A. Minor, A. Alivisatos, U. Dahmen, Nano Lett. 9 (6) (2009) 2460–2465.
[45] B. Fritsch, A. Hutzler, M. We, S. Khadivinazar, L. Vogl, M. Jank, M. März, E. Spiecker, Nanoscale Adv. 3 (9) (2021) 2466.
[46] A. Ashffag, J. An, P. Ulanski, A. Mohamad, Pharmaceutics 13 (11) (2021) 1765.
[47] P. Ulanski, I. Janik, J. Rosiak, Radiat. Phys. Chem. 56 (1–6) (1998) 289.
[48] J. Ulanski, P. Rosiak, Nucl. Instrum. Methods Phys. Res. B: Beam Interact. Mater. At. 151 (1–4) (1999) 356.
[49] P. Ulanski, S. Kadlubowski, J. Rosiak, Radiat. Phys. Chem. 63 (3–6) (2002) 533.
[50] H. Schwarz, R. Dodson, J. Phys. Chem. 93 (1) (1989) 409.
[51] G. Dey, K. Kishore, Radiat. Phys. Chem. 72 (5) (2005) 565.
[52] J. Korpanty, L. Parent, H.N., S. Weigand, N. Gianneschi, Nat. Commun. 2021, 12 6568.
[53] M.J. Meijerink, C. Spiga, T.W. Hansen, C.D. Damsgaard, K.P. de Jong, J. Zečević, Part. Part. Syst. Charact. 36 (1) (2019) 1.
[54] M. Karg, S. Wellbert, I. Pastoriza-Santos, A. Lapp, L. Liz-Marzán, T. Hellweg, Phys. Chem. Chem. Phys. 10 (44) (2008) 6708.
[55] S. Shahabi, L. Treccani, K. Rezwan, J. Nanopart. Res. 17 (6) (2015) 270.
[56] C. Graf, D.L.J. Vossen, A. Imhof, A. van Blaaderen, Langmuir 19 (2003) 6693.
[57] J. Fokkema, J. Fermie, N. Liv, D. van den Heuvel, T. Konings, G. Blab, A. Meijerink, J. Klumperman, H. Gerritsen, Sci. Rep. 8 (2018) 13625.
[58] A. Verch, M. Pfaff, N. de Jonge, Langmuir 31 (25) (2015) 6956.